Analytical Chemistry

Chemoselective Detection of 2,4,6-trinitrophenol by Ground State Adduct Formation via Protonation of Quinoline Moiety of Non-heme Ligands with Structural Evidence

Sarvesh S. Harmalkar, Ankita V. Naik, Madhuri K. Nilajakar, and Sunder N. Dhuri*[a]

Dedicated to Professor S.K. Paknikar on the occasion of his 85th birthday

Four quinoline based non-heme tetradendate ligands *viz. N,N′*-di(quinolin-8-yl)ethane-1,2-diamine ($BQENH_2$) **1**, *N,N′*-di(quinolin-8-yl)propane-1,3-diamine **2** ($BQPNH_2$), *N,N′*-di(quinolin-8-yl) butane-1,4-diamine ($BQEBNH_2$) **3** and *N,N′*-di(quinolin-8-yl) hexane-1,6-diamine ($BQEHNH_2$) **4** are structurally characterized and used in selective detection of 2,4,6-trinitrophenol (TNP) with high quenching constants. The plausible reaction mechanism involves ground state protonation of quinoline nitrogen atoms in compounds **1–4** by TNP with formation of picrate adducts (**1a-4a**). The protonation of **1–4** is confirmed by infrared, ^{1}H-NMR spectroscopies, powder XRD and the single crystal structure analysis of **1a** and **4a**. Crystal structures further infer that after protonation, **1a** and **4a** are stabilized by intramolecular hydrogen bonding.

Introduction

In modern days the selective detection of explosives in a mixture of other compounds is an area of active research due to the increased use of these materials in global terrorism. The nitroaromatic compounds (NACs) such as nitrophenols (NP), nitrobenzenes (NB) and nitrotoluenes (NT) have been widely used as explosives.[1] These organic compounds are known for their high explosivity and toxicity, thus becoming serious threats to human health, environment and social security.[2] A well-known explosive chemical with low safety coefficient and high explosive detonation is 2,4,6-trinitrophenol (TNP) commonly known as picric acid (PA).[3] The explosive TNP is highly soluble in water and its remains are difficult to separate out from other effluents thus creating water pollution. This is one of the reasons as to why researchers are working on the selective detection of such detonating substances to provide immediate remedy to the human health and socio-economic problems.[4] Although many techniques are known in literature for the detection of TNP, the optical methods have been widely employed due to its easy accessibility, simple instrumentation and detection at lower concentrations. In chromo-fluorogenic probes, the detection of electron deficient NACs is carried out using electron rich fluorophores such as fluorescent conjugated polymers like poly(phenyleneethyny-lene)s, polyphenylene-vinylenes, silicon containing polymers, molecularly imprinted polymers (MIPs), single fluorophores *viz* polycyclic aromatic hydrocarbons, heterocycles and metal organics.[5] Substituted heme compounds namely *meso*-tetra(4-sulfonatophenyl)porphyrin and *meso*-tri(4-sulfonatophenyl)-mono(4-carboxyphenyl) porphyrin were used in the fluorescence detection of trinitrotoluene (TNT).[5] Knapp *et al* have reported a family of Zn-salen based compounds for the fluorescence detection of various NACs.[6] Recently, selective sensing of TNP in an aqueous medium using iridium(III) compounds was attributed to the O–H···O interactions between TNP and the ancillary ligand in graphitic carbon nitride nanosheets using X-ray crystallography.[7] A functionalized reduced graphene oxide has shown high selectivity in TNP detection.[8] Metal organic frameworks (MoFs) containing fluorophores are known as sensors for various ntiropheol derivatives.[9]

A wide number of free ligands such as imidazole derivatives and 4,40-(9,9-dimethylfluorene-2,7-diyl)dibenzoic has shown high sensitivity towards TNP detection.[10] Rao *et al* have used tetrapyrenyl calix[4]arene conjugate moiety[11] while Das and coworkers have reported newly designed azo-polymer in TNP detection.[12] A hemicyanine dye bearing conjugated 4-(dimethylamino)benzaldehyde based fluorophores are known for its valuable property of sensing TNP.[13] A large number of quinoline based compounds are also proven to be effective as fluorophores in TNP detection.[14] Britovsek *et al* in their work have investigated the effect of ligand topology on the field strength of non-heme iron(II) catalyzed reactions by using different bis(quinolyl) based tetradentate ligands (Scheme S1).[15] Using a known synthetic strategy, we have reported few quinoline based N-donor ligands and their transition metal compounds, $[M(L)(H_2O)_2]^{2+}$ where M = divalent Co, Ni, Cu cations and L = N^1,N^2-dimethyl-N^1,N^2-di(quinolin-8-yl) ethane-1,2-diamine ($BQENMe_2$), N^1,N^2-dimethyl-N^1,N^2-di(quino-

[a] S. S. Harmalkar, A. V. Naik, M. K. Nilajakar, Dr. S. N. Dhuri
School of Chemical Sciences, Goa University, Goa 403206
E-mail: sndhuri@unigoa.ac.in

Supporting information for this article is available on the WWW under https://doi.org/10.1002/slct.202002244

lin-8-yl)cyclohexane-1,2-diamine ($BQCNMe_2$), N^1,N^2-di(quinolin-8-yl)ethane-1,2-diamine ($BQENH_2$) and N^1,N^2-di(quinolin-8-yl) cyclohexane-1,2-diamine ($BQCNH_2$) with their roles in catalytic reactions and antibacterial studies in our earlier work.[16] Herein, we are reporting the fully characterized four quinoline based tetradendate N-donor ligands (**1**-**4**) (Figure 1) in the chemo selective sensing of nitroaromatic compounds. Efforts are made to postulate the mechanism of fluorescence quenching using spectroscopic and structural evidences.

Results and Discussion

Four ligands (**1**-**4**) were prepared in large yields using a modified Bucherer procedure reported by Britovsek *et al* as well as by our group.[15,16] In this method, the diamines namely 1,2-diaminoethane (en), 1,3-propanediamine (1,3-pn), 1,4-butanediamine (1,4-bn) and 1,6-hexanediamine (1,6-hn) were reacted with 8-hydroxy quinoline under refluxing conditions in aqueous medium for nearly eight days to obtain the desired ligands **1–4** (Scheme 1). The infrared (IR) spectra of all four compounds exhibit a sharp peak in the region, 3400–3300 cm^{-1} which is attributed to the N–H stretching vibration (Figure S1). UV-Visible spectra of **1–4** in CH_2Cl_2 exhibit two intense bands at 259 and 370 nm with a shoulder band at 335 nm. A band at 259 nm is assigned to π-π* transition corresponding to the conjugation within quinoline moieties of **1–4** (Figure S2). A shoulder band at 335 nm and a broad band at 370 nm is attributed to the n-π* transition originating from the non-bonded electrons of nitrogen atoms and the conjugated quinoline rings. All four ligands are characterized by ^1H and ^{13}C-NMR and the chemical shifts observed here are in good agreement with those expected for compounds **1–4** [Figure S3-S6].

For the first time all four compounds were grown as single crystals and characterized by single crystal X-ray diffractometry. The crystal structures of **1–4** are depicted in Figure 1. Compounds **1** and **4** crystallize in a centrosymmetric monoclinic space group $P2_1/n$ while **2** and **3** crystallizes in C_2/c and $P2_1/c$ respectively [Table S1]. The careful structure analysis reveal that in compound **1** the one-dimensional chains are formed along the crystallographic *b*-axis which are resulting from the intermolecular π···π interactions between the adjacent quinoline rings (Figure S7). These chains are crossed linked with C–H···N intermolecular hydrogen bonding with C···N distance of 3.955 Å (C–H···N at an angle of 148.99°) (Table S2). The quinoline nitrogen atom N1 act as acceptor in C-H···N

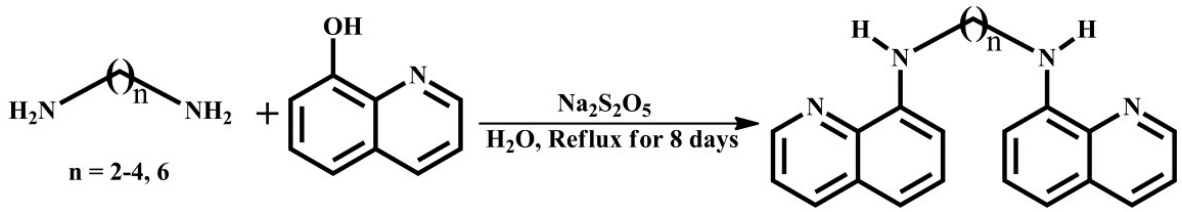

Scheme 1. Synthetic stratergy employed for the preparation of ligands **1–4**.

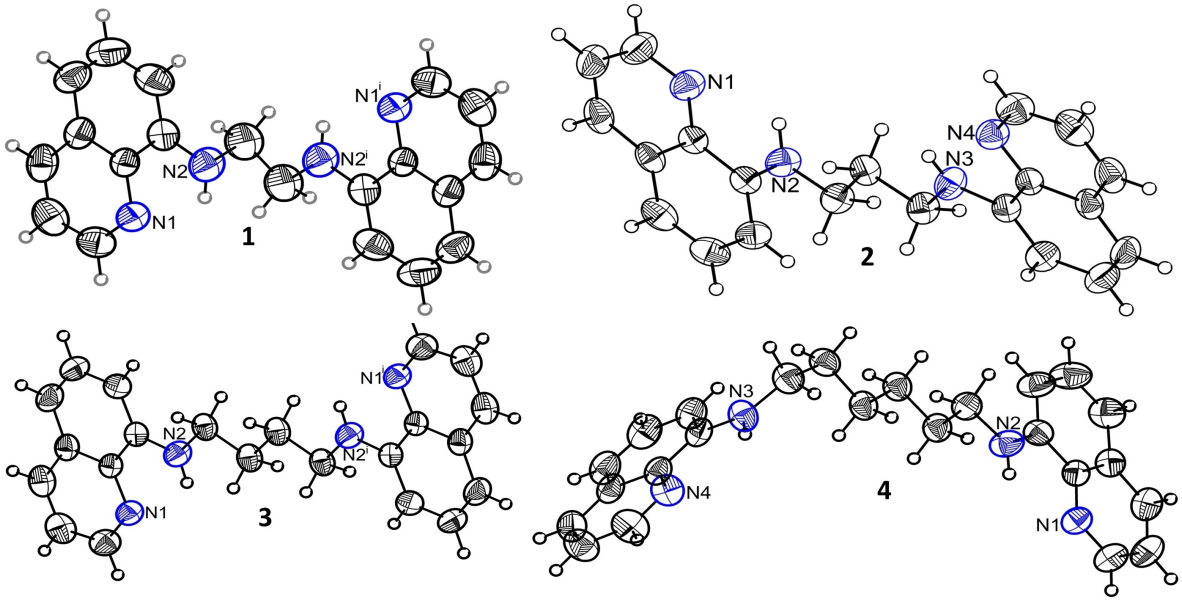

Figure 1. Crystal structures of **1–4**. Displacement ellipsoids are drawn at 50% probability level for all atoms excepting the hydrogens which are shown as circles of arbitrary radii. For **1** and **3** symmetry codes are given in supplimentary material.

intermolecular hydrogen bonding. In compound **2**, each molecule is surrounded by four other molecules resulting from C-H···π interactions (Figure S8b). These interactions thus run in a *zig-zag* pattern in a crystal packing lattice (Figure S8c). Like compound **1**, again the one-dimensional chains resulting from intermolecular π···π and C–H···π interactions between the adjacent quinoline rings are running along the crystallographic *a*-axis in the crystal structure of **3** (Figure S9b). These chains are further interconnected with C–H···N interactions and each molecule of **3** is surrounded by four of its other molecules resulting from C–H···N (Figure S9c). The crystal structure of compound **4** shows that it exhibits a bent L shaped structure with one quinoline ring being at an angle of ~110° due to the long hexane chain [Figure S10].

The molecules of **4** forms the two one dimensional chains extending in the opposite directions when viewed along the crystallographic *c*-axis resulting from the intermolecular C–H···π with a distance of 2.888 Å between the H atom and the centroid of the ring (Figure S10). These chains are then interlinked with C–H···π and C–H···N interactions.

As UV-Visible spectra of compounds **1–4** exhibited bands at $\lambda_{max} = 259$, 335 and 370 nm, we thought of investigating the photoluminescence properties of these compounds. On exciting compounds **1–4** at 259 nm wavelength, we could not observe any a fluorescence emission, on other hand, the excitation at 335 and 370 nm showed fluorescence response centered at λ_{max} of 474 nm for all four compounds **1–4**. This fluorescence property of **1–4** propagated us to further investigate their use in the detection of nitroaromatic compounds (NACs).

Before starting this investigation, we first decided to confirm the bulk and the single crystal phase purity of **1–4**. To do so, the X-ray powder patterns of compound **1–4** were recorded and compared with the simulated powder patterns of **1–4** obtained from their crystal structure data (Figure S11). On comparison of these two data, it was observed that the experimental and simulated powder patterns of **1–4** were nearly matching suggesting the phase purity of bulk and single crystal composition of **1–4** (Figure S11). With the confirmation of phase purity, we then investigated an emissive response of series of suspensions of **1–4** in ethanol solution containing NACs such as nitrobenzene (NB), *p*-nitrotoluene (PNT) and *p*-nitrophenol (PNP) (Figure S12). The significant quenching of 474 nm band intensity was observed on treating PNP with **1–4** in comparison with NB and PNT compounds. The quenching observed at 335 nm excitation was much greater than that observed at 370 nm. With high sensitivity of **1–4** towards PNP compared to other NAC's, we then decided to check the selectivity of PNP over other phenol derivative compounds namely *p*-bromophenol (PBP), *p*-aminophenol (PAP), phloroglucinol (PG), resorcinol(R) and *4*-hydroxybenzaldehyde (HBA). The spectral intensities of 474 nm band of **1–4** in the presence of these phenols clearly suggested that only PNP is better candidate in quenching the emission of **1–4** at both the excitations (335 and 370 nm) revealing its higher selectivity over the other derivatives (Figure S13).

Since PNP showed a good selectivity so far, its quenching efficiency was then compared with related nitrophenol derivatives *viz o*-nitrophenol (ONP), *m*-nitrophenol (MNP), *2,4*-dinitrophenol (DNP) and *2,4,6*-trinitrophenol (TNP). All the nitrophenol derivatives showed drastic quenching in the intensity at 474 nm (Figure 2 and Figure S14). A comparative study of the quenching efficiencies of nitrophenols showed a following order of quenching: MNP < ONP < PNP < DNP < TNP at both excitations (335 and 370 nm) and this order is in good agreement with the acidity of phenol derivatives. TNP showed fluorescence quenching of 79(±2), 77(±2), 80 (±2) and 76 (±3) % for compounds **1, 2, 3** and **4** respectively with their corresponding quenching effect coefficients of 36.5 x 10^3, 33.8 x 10^3, 39.3 x 10^3 and 32.2 x 10^3 at excitation of 335 nm. On excitation at 370 nm, the fluorescence quenching yields were 87(±2), 86(±1), 88(±2) and 86(±2) % respectively for compounds **1**, **2**, **3** and **4** and these values are slightly higher compared to excitation at 335 nm. Interestingly, on other hand the quenching effect coefficients were almost doubled (67.6 x 10^3, 60.3 x 10^3, 74.2 x 10^3 and 62.2 x 10^3 for compounds **1–4** respectively) with 0.1 mM concentration at 370 nm excitation (Figure 2). This result indicate that 370 nm excitation is much better for the quenching fluorescence of **1–4** by TNP over 335 nm. The digital photographs showing quenching of fluorescence emission of **1–4** by TNP at 370 nm are shown in Figure 3.

The selectivity of TNP over other nitrophenol derivatives was studied by comparing their quenching percentages with that of TNP at both the excitations. It was observed that quenching percentages due to the other nitrophenols derivatives range from 30–61% at 335 nm excitation, while the quenching percentages range from 19–33% at 370 nm excitation with intensities lying in a narrow range (Figure 2, Figure S14). The present data unambiguously suggest that compounds **1–4** can be thus selectively used as the chemical sensing reagents in the detection of TNP from the mixture of nitrophenol derivatives at 370 nm.

In the literature, the several mechanisms which include photo-induced electron transfer (PET), resonance energy transfer (RET), electron exchange (EE) or Dexter interactions (DI) and intramolecular charge transfer (ICT) are reported in the quenching reaction by TNP.[17] Based on our results, we initially thought that a probable mechanism could be a well-known RET process wherein an energy is transferred from the excited fluorophore to the electron deficient TNP acceptor. To check whether RET step occur in emission process, we then investigated the spectral overlap of the absorption band of TNP acceptor and the emission band of the donor compounds (**1**-**4**) (Stoke's Shift) [Fig S15]. The absorption-emission response indeed showed some overlap of the bands which led us to infer that RET step may be responsible for the fluorescence quenching behavior as reported in the literature.[18] However, it is also reported that RET depends not only on the spectral overlap but also on other factors like dipole interaction, intermolecular distance between the acceptor and the donor[19] and the overlap was not of a significant amount. To further investigate the mechanistic dilemma of the quenching process,

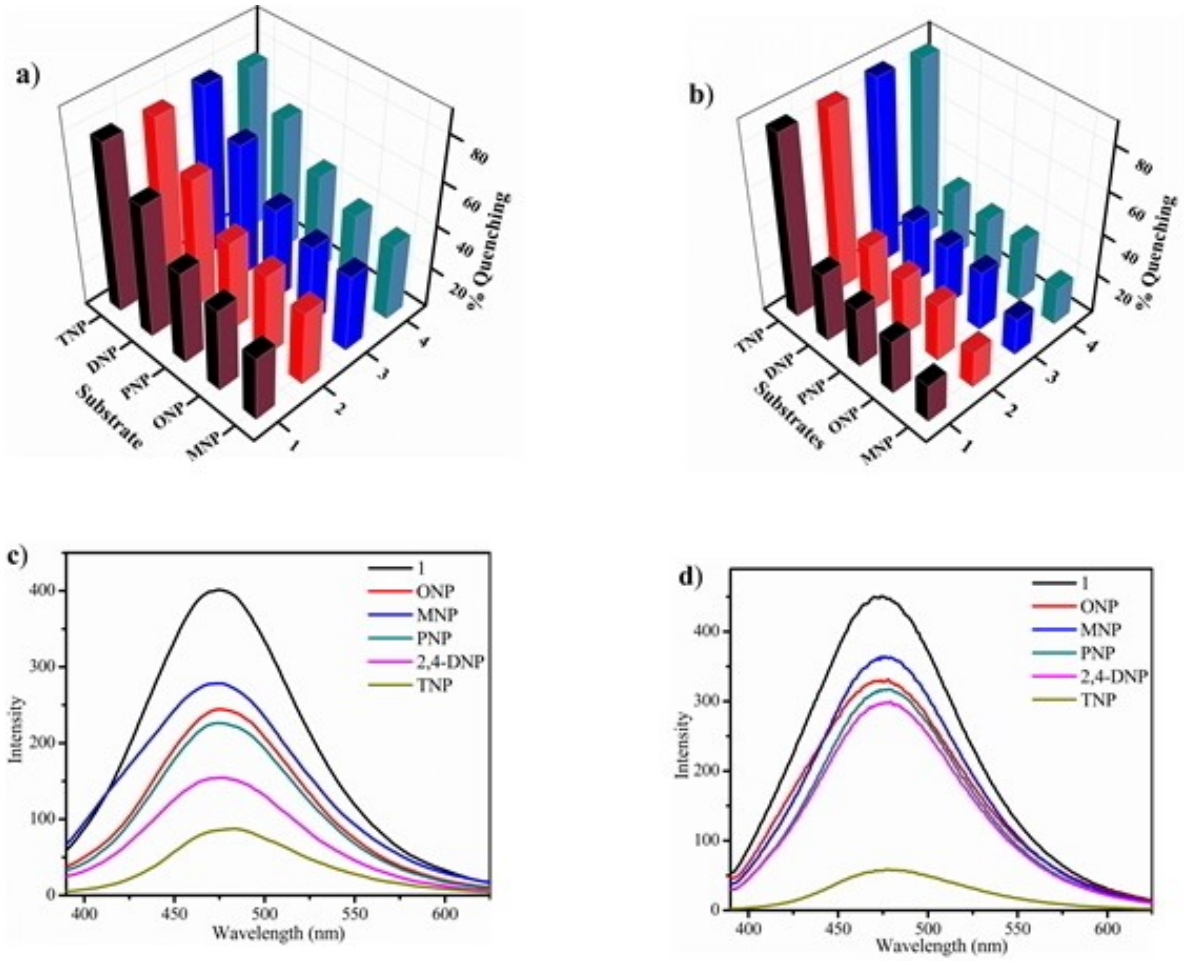

Figure 2. Fluorescent quenching percentages of ethanol suspensions of compounds 1–4 with 100 μM different analytes (slits: 20 nm/20 nm) (a) λex = 335 nm (b) λex = 370 nm.

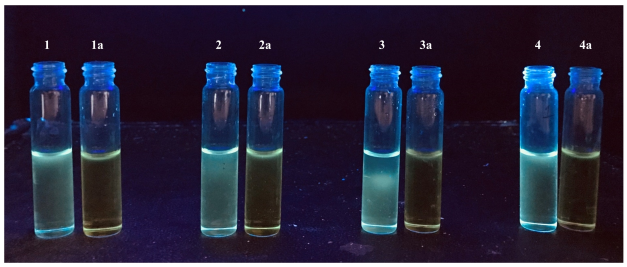

Figure 3. Digital pphotograph showing the fluorescence showed by the solution of compound **1–4** in comparison to that shown on addition of 2eq of TNP solution under UV radiation of 370 nm.

we then performed the titration experiments wherein 15 μL of 0.1 mM TNP solution was added to 100 μM ethanolic suspension (3 mL) of **1–4** in increments. With increasing concentration of TNP up to 200 μM, the fluorescence intensity was diminished with nearly 96 % of quenching at 370 nm (Figure S16). This result also revealed that the stoichiometry of 1:2 of ligand to TNP is prerequisite in this quenching process. To gain more insights in the mechanistic and stoichiometry aspects, we then decided to perform the reaction of compounds **1–4** with TNP at higher concentrations with a ratio of 1:2 (ligand : TNP) under the identical experimental conditions as used in fluorescence quenching experiments. About 200 μL of 0.1 M **1–4** in DMSO was added to 2 mL ethanol and to this 200 μL 0.2 M solution of TNP in DMSO was added. In all the four reactions of **1–4** with TNP an orange insoluble crystalline precipitate was immediately thrown out. This was a first indication of the formation of a salt between an amine and a picric acid (TNP). The orange solids (**1a–4a**) obtained in the reaction of **1–4** and TNP were isolated, properly vacuum dried and then characterized by IR spectra and ^{1}H-NMR spectra using DMSO-d_6 solvent. The IR and ^{1}H-NMR of **1** and **1a** are shown in Figure 4 while IR and ^{1}H-NMR spectra of the remaining compounds (**2a-4a** compared with those **2–4**) are shown in Figure S17 and S18. IR spectra of **1** and **1a** clearly showed the distinct spectral features in the region 3400–3000 cm^{-1} attributed to the protonation of **1** (Figure 4a). Further, a broadening of N–H stretching vibration in **1a** indicates that in **1a** the cation and anion is held together by weak H-bonding interactions (*vide infra*). Similar broadening trends were also observed in the IR spectra **2a-4a** when

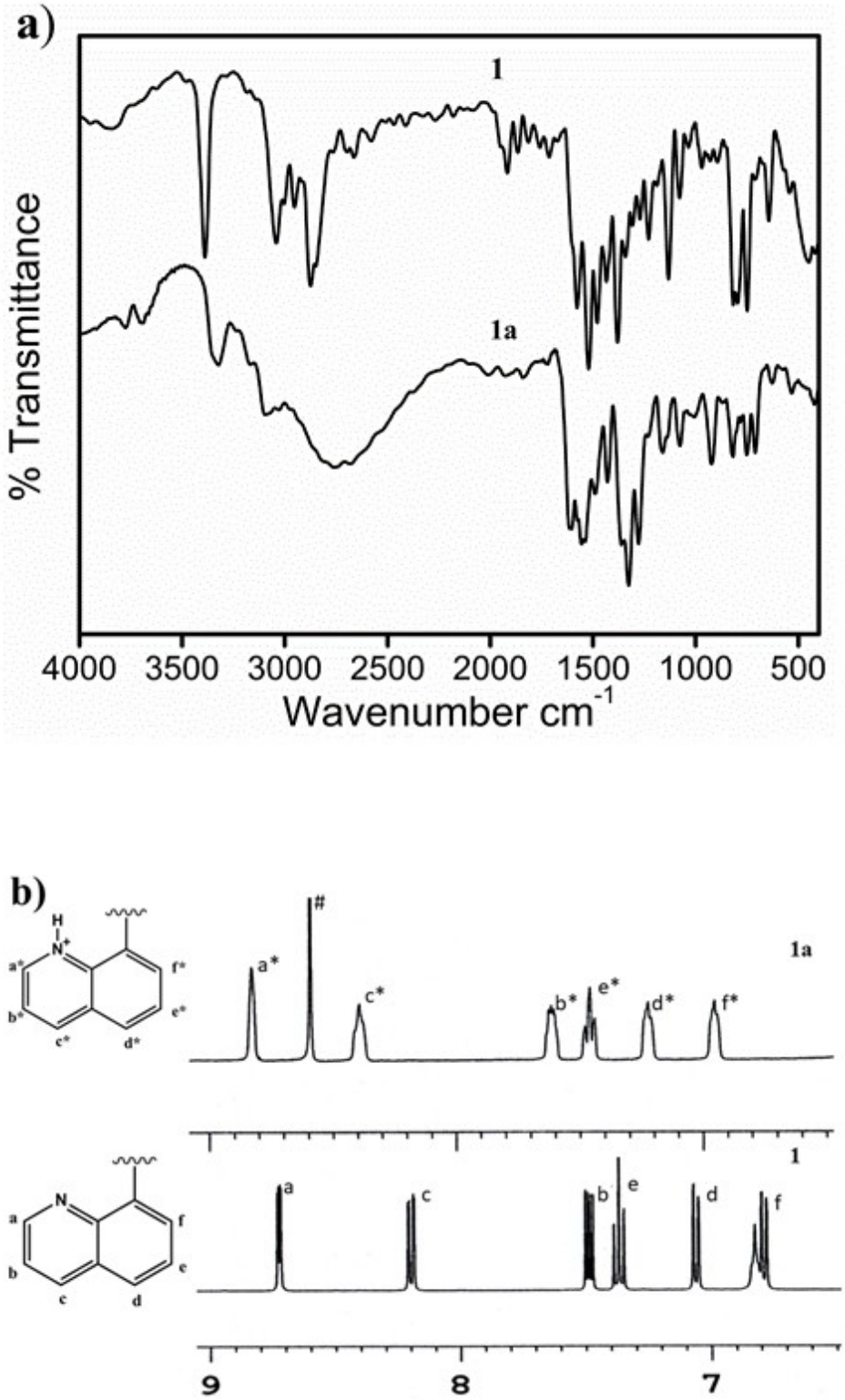

Figure 4. (a) IR spectra of **1** and **1 a** recorded in KBr matrix. (b) ^{1}H-NMR spectra of **1** and **1 a** in DMSO-d_6 showing the signals due to quinoline protons (*peak due to protons of TNP).

compared with the IR spectra of **2–4** (Figure S17). The careful interpretation of the ^{1}H-NMR spectrum of **1 a** revealed that there is a downfield of chemical shift (δ) values of the quinoline protons as compared to the δ values of the protons in **1** (Figure 4b). This observation is thus attributed to effect of protonation of the quinoline N on its neighbouring protons.[20]

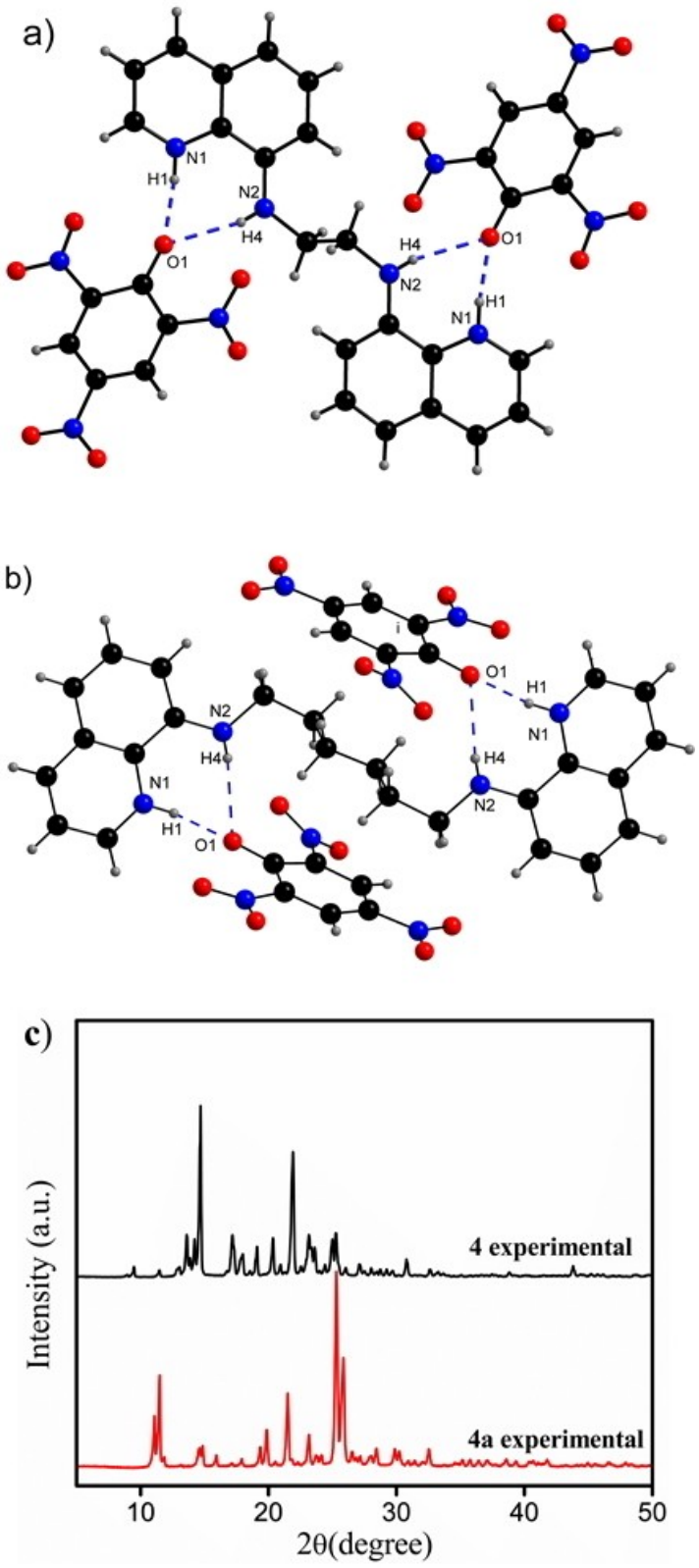

Figure 5. (a) Crystal structure **1 a**; (b) crystal structure of **4 a**. Hydrogen bonding interactions are shown as broken lines. (c) PXRD patterns on **4** and **4 a**.

Additionally, a new peak observed was attributed to the protons of picrate anions. Similar observations in the ^{1}H-NMR spectra of **2 a**-**4 a** were also observed suggesting the protonation of ligands **2**–**4** to form picrate salts (Figure S18).

Finally, to understand the structural aspects of resultant products of reactions of **1–4** with TNP, we tried to crystalize **1a**-**4a** in different solvents. Our efforts resulted in growing the single crystals of only compounds **1a** and **4a** in DMSO:ethanol (1:1) mixture while **2a** and **3a** were only obtained in powder form. The crystals structures of **1a** and **4a** are shown in Figure 5 (a,b). It is clearly seen from structures of **1a** and **4a** that there is protonation of two quinoline nitrogen atoms forming a dication and the two TNP molecules behaving as picrate anions formally satisfying the stoichiometry of 1:2 of ligand to TNP.

The quinolinium cation and pictrate anions are held together by weak hydrogen bonding interactions originating from quinolinium nitrogen N1-H1···O1 picrate in **1a** and **4a**. The intramolecular hydrogen bonding is thus in accordance with IR spectra of **1a** which showed broadening of N–H stretching vibration compared to the N–H stretching vibration of **1** (*vide supra*) (Figure S17). Finally, PXRD patterns of **1a** and **4a** were also recorded and compared with their simulated powder patterns obtained from their structures to check their single crystal and bulk phase purity (Figure S19). A comparison of PXRD patterns of **1** and **1a** revealed that they are altogether different compounds further supporting protonation of **1**. Figure 5c shows a comparative PXRD patterns of **4** and **4a** deducing the clarity that **4a** is protonated.

In the literature, it is reported that a TNP molecule and a fluorophore comes in only close proximity without protonation of a fluorophore and deprotonation of TNP, instead their close proximity is attributed only to the weak O–H···N hydrogen bonding interactions.[7] In the present case of **1a** and **4a**, the trend is reverse, where now we see N–H···O interactions originating from protonated quinoline (quinolinium cation) and picrate anions. Since these reactions were carried out without excitation we propose that the reaction of **1–4** with TNP results in the ground state protonation followed by the formation H-bonded cation-anion dipole pair. This mechanism falls in the category of static quenching which states that a ground state complex is formed between the fluorophore and the quencher which itself is non-fluorescent and thereby resulting in quenching of the fluorescence emission.[21] Our case also results in the formation of a ground state adduct between the compounds **1–4** and TNP which is also non-fluorescent however the process involves a proton transfer step prior to the adduct formation. We therefore say that a modified static quenching mechanism is more appropriate in this case.

After protonation, since quinoline N has a positive charge it tries to pull the electron density of the quinoline ring towards itself thereby disturbing the conjugation of the quinoline ring which ultimately leads to the decreased fluorescence intensity of the compounds. This hypothesis is contradicting the hypothesis presented by other research groups, who have used different quinoline based compounds in the sensing of TNP.[18,22] The mechanism earlier proposed was RET from the excited compound to the electron deficient acceptor (TNP) based on the common overlapping in emitted energy of the compound with absorption energy of TNP. Our work however showcases that protonation of the quinoline N followed by adduct formation results in the decrease in the fluorescence intensity and we believe that in all quinoline based compounds the fluorescence quenching mechanism would also occur similarly. Our group is presently investigating more such compounds in the fluorescence quenching mechanisms.

Conclusion

Four fluorescent compounds **1–4** were synthesized by a simple modification of Bucherer reaction and were characterized using spectroscopic and single crystal XRD. These compounds were investigated in the sensing of nitrophenols. All four compounds showed promising results with high sensitivity for TNP explosive compared to other nitrophenols. All four compounds gave proficiently high quenching constants ($> 32 \times 10^3$ at $\lambda_{ex} =$ 335 nm and $> 60 \times 10^3$ at $\lambda_{ex} = 370$ nm) suggesting that these compounds can be used as promising sensors for the detection of TNP. A modified static quenching mechanism have been proposed in the quenching of fluorescence of **1–4** by TNP.

Supporting Information Summary

This experimental section, characterization and emission spectra are available in Supporting Information.

Acknowledgements

We gratefully acknowledge Council of Scientific and Industrial Research (CSIR), New Delhi, India (No. 01(2923)/18/EMR-II) for financial support and thank Dr. Sandeep Kumar Dey for useful discussions.

Conflict of Interest

The authors declare no conflict of interest.

Keywords: Chemoselective · Fluorescence · Quenching · TNP · Explosives · Crystal structures · Protonation · Static Quenching.

[1] a) D. Badgujar, M. Talawar, S. Asthana, P. Mahulikar, *J. Hazard. Mater.*, **2008**, *151*, 289–305; b) D. S. Moore, *Rev. Sci. Instrum.* **2004**, *75*, 2499–2512.
[2] a) E. R. Travis, N. C. Bruce, S. J. Rosser, *Environ. Pollut.* **2008**, *153*, 119–126; b) E. A. Naumenko, B. Ahlemever, E. Baumgart-Vogt, *Environ. Toxicol.* **2017**, *32*, 989–1006; c) T. M. Mallon, J. M. Ortiz, W. H. Candler, G. Rogers, R. Hillburn, *Mil. Med.* **2014**, *179*, 1374–1383.
[3] a) T. F. Jenkinson, C. L. Grant, G. S. Brar, P. G. Thorne, P. W. Schumacher, T. A. Ranney, *Field Anal. Chem. Technol.* **1997**, *1*, 151–163; b) J. Shen, J. Zhang, Y. Zuo, L. Wang, X. Sun, J. Li, W. Han, R. He, *J. Hazard. Mater.* **2009**, *163*, 1199–1206; c) E. H. Volwiler, *Ind. Eng. Chem.* **1926**, *18*, 1336–1337.
[4] a) B. Joarder, A. V. Desai, P. Samanta, S. Mukherjee, S. K. Ghosh, *Chem. Eur. J.* **2015**, *21*, 965–969; b) K. M. Wang, L. Du, Y. L. Ma, Q. H. Zhao, *Inorg. Chem. Commun.* **2016**, *68*, 45–49; c) Y. Deng, N. Chen, Q. Li, X. Wu, X. Huang, Z. Lin, Y. Zhao, *Cryst. Growth Des.* **2017**, *17*, 3170–3177.
[5] a) Y. Salinas, R. Martinez-Manez, M. D. Marcos, F. Sancenon, A. M. Castero, M. Parra, S. Gilad, *Chem. Soc. Rev.* **2012**, *41*, 1261–1296; b) M. Rahman, H. J. Harmon, *Spectrochim. Acta Part A* **2006**, *65*, 901–906; c) W. M. Hikal, H. J. Harmon, *J. Hazard. Mater.* **2008**, *154*, 826–831.
[6] a) M. E. Germain, T. R. Vargo, P. G. Khalifah, M. J. Knapp, *Inorg. Chem.* **2007**, *46*, 4422–4429; b) M. E. Germain, M. J. Knapp, *J. Am. Chem. Soc.*

2008, *130*, 5422–5423; c) M. E. Germain, T. R. Vargo, B. A. McClure, J. J. Rack, P. G. Van Patten, M. Odoi, M. J. Knapp, *Inorg. Chem.* **2008**, *47*, 6203–6211.
[7] W. Che, G. Li, X. Liu, K. Shao, D. Zhu, Z. Su, M. R. Bryce, *Chem. Commun.* **2018**, *54*, 1730–1733.
[8] D. Dinda, A. Gupta, B. K. Shaw, S. Sadhu, S. K. Saha, *ACS Appl. Mater. Interfaces* **2014**, *6*, 10722–10728.
[9] a) B. Parmar, K. K. Bisht, Y. Rachuri, E. Suresh, *Inorg. Chem. Front.* **2020**, *7*, 1082–1107; b) J. Wang, J. Wu, L. Lu, H. Xu, M. Trivedi, A. Kumar, J. Liu, M. Zheng, *Front. Chem.* **2019**, *7*, 1–9; c) Q. Chen, J. Cheng, J. Wang, L. Li, Z. Liu, X. Zhou, Y. You, W. Huang, *Sci. China Chem.* **2019**, *62*, 205–211; d) S. S. Nagarkar, A. V. Desai, P. Samanta, S. K. Ghosh, *Dalton Trans.* **2015**, *44*, 15175–15180.
[10] a) H.-L. Ding, L.-D. Chen, N. Wang, K. Li, Y. An, C.-W. Lü, *Talanta* **2019**, *195*, 345–353; b) J. C. Ni, J. Yan, L. J. Zhang, D. Shang, N. Du, S. Li, J. X. Zhao, Y. Wang, Y. H. Xing, *Tetrahedron Lett.* **2016**, *57*, 4978–4982.
[11] S. K. Dinda, M. A. Hussain, A. Upadhyay, C. P. Rao, *ACS Omega* **2019**, *4*, 17060–17071.
[12] M. Ansari, R. Bera, S. Mondal, N. Das, *ACS Omega* **2019**, *4*, 9383–9392.
[13] N. Nagamani, S. Lakshmanan, D. Govindaraj, C. Ramamoorthy, N. Ramalakshmi, S. A. Antony, *Spectrochim. Acta Part A* **2019**, *207*, 321–327.
[14] a) S. Halder, P. Ghosh, A. Hazra, P. Banerjee, P. Roy, *New J. Chem.* **2018**, *42*, 8408–8414; b) C. Gogoi, S. Biswas, *Dalton Trans.* **2018**, *47*, 14696–14705; c) Y. Ma, H. Li, S. Peng, L. Wang, *Anal. Chem.* **2012**, *84*, 19, 8415–8421.
[15] J. England, G. J. P. Britovsek, N. Rabadia, A. J. P. White, *Inorg. Chem.* **2007**, *46*, 3752–3767.
[16] a) D. D. Narulkar, A. R. Patil, C. C. Naik, S. N. Dhuri, *Inorg. Chim. Acta* **2015**, *427*, 248–258; b) S. S. Harmalkar, D. D. Narulkar, R. J. Butcher, M. S. Deshmukh, A. K. Srivastava, M. Mariappan, P. Lama, S. N. Dhuri, *Inorg. Chim. Acta* **2019**, *486*, 425–434; c) D. D. Narulkar, A. K. Srivastava, R. J. Butcher, S. N. Dhuri, *J. Struct. Chem.* **2018**, *59*, 1168–1175; d) S. S. Harmalkar, R. J. Butcher, V. V. Gobre, S. K. Gaonkar, L. R. D'Souza, M. Sankaralingam, I. Furtado, S. N. Dhuri, *Inorg. Chim. Acta* **2019**, *498*, 1190202, 1–11.
[17] a) H.-Y. Mi, J.-L. Liu, M.-M. Guan, Q.-W. Liu, Z.-Q. Zhang, G.-D. Feng, *Talanta* **2008**, *187*, 314–320; b) A. S. Tanwar, L. R. Adil, M. A. Afroz, P. K. Iyer, *ACS Sens.* **2018**, *3*, 1451–1461; c) D. C. Santra, M. K. Bera, P. K. Sukul, S. Malik, *Chem. Eur. J.* **2016**, *22*, 2012–2019.
[18] K. Jianga, S.-H. Luoa, C.-M. Panga, B.-W. Wanga, H.-Q. Wua, Z.-Y. Wanga, *Dyes Pigm.* **2019**, *162*, 367–376.
[19] a) F. Perrin, *Ann. Phys.* **1932**, *10*, 283–314; b) H. Kallmann, F. London, *Z. Phys. Chem.* **1929**, *2B*, 207; c) T. Förster, *Naturwissenschaften*, **1946**, *33*, 166–175.
[20] a) S. K. Dey, A. Pramanik, G. Das, *CrystEngComm* **2011**, *13*, 1664–1675; b) S. K. Dey, G. Das, *Cryst. Growth Des.* **2011**, *11*, 4463–4473.
[21] X. Sun, Y. Wang, Y. Lei, *Chem. Soc. Rev.* **2015**, *44*, 8019–8061.
[22] S. Halder, P. Ghosh, A. Hazra, P. Banerjee, P. Roy, *New J. Chem.* **2018**, *42*, 8408–8414.

Submitted: June 4, 2020
Accepted: July 10, 2020